HHS Public Access

Author manuscript

Adv Healthc Mater. Author manuscript; available in PMC 2024 October 01.

Published in final edited form as:

Adv Healthc Mater. 2023 October ; 12(25): e2300587. doi:10.1002/adhm.202300587.

Rational Design and Efficacy of Glucose-Responsive Insulin Therapeutics and Insulin Delivery Systems by Computation using Connected Human and Rodent Models

Sungyun Yang,
Department of Chemical Engineering, Massachusetts Institute of Technology, Cambridge, MA 02139, USA

Jing Fan Yang,
Department of Chemical Engineering, Massachusetts Institute of Technology, Cambridge, MA 02139, USA

Xun Gong,
Department of Chemical Engineering, Massachusetts Institute of Technology, Cambridge, MA 02139, USA

Michael A. Weiss,
Department of Biochemistry and Molecular Biology, Indiana University of Medicine, Indianapolis, IN 46202, USA

Michael S. Strano
Department of Chemical Engineering, Massachusetts Institute of Technology, Cambridge, MA 02139, USA

Abstract

Glucose-responsive insulins (GRIs) use plasma glucose levels in a diabetic patient to activate a specifically designed insulin analogue to a more potent state in real time. Alternatively, some GRI concepts use glucose-mediated release or injection of insulin into the bloodstream. GRIs hold promise to exhibit much improved pharmacological control of the plasma glucose concentration, particularly for the problem of therapeutically induced hypoglycemia. Several innovative GRI schemes have been introduced into the literature, but there remains a dearth of quantitative analysis to aid the development and optimization of these constructs into effective therapeutics. In this work, we evaluate several classes of GRIs that have been proposed using a pharmacokinetic model we previously described, PAMERAH, simulating the glucoregulatory system of humans and rodents. We group GRI concepts into three mechanistic classes: (1) intrinsic GRIs, (2) glucose-responsive particles, and (3) glucose-responsive devices. Each class is analyzed for optimal designs that maintain glucose levels within the euglycemic range. These derived GRI parameter spaces are then compared between rodents and humans, providing the differences in clinical translation success for each candidate. This work demonstrates a computational

strano@mit.edu .

Supporting Information
Supporting Information is available from the Wiley Online Library.

framework to evaluate the potential clinical translatability of existing glucose-responsive systems, providing a useful approach for future GRI development.

Graphical Abstract

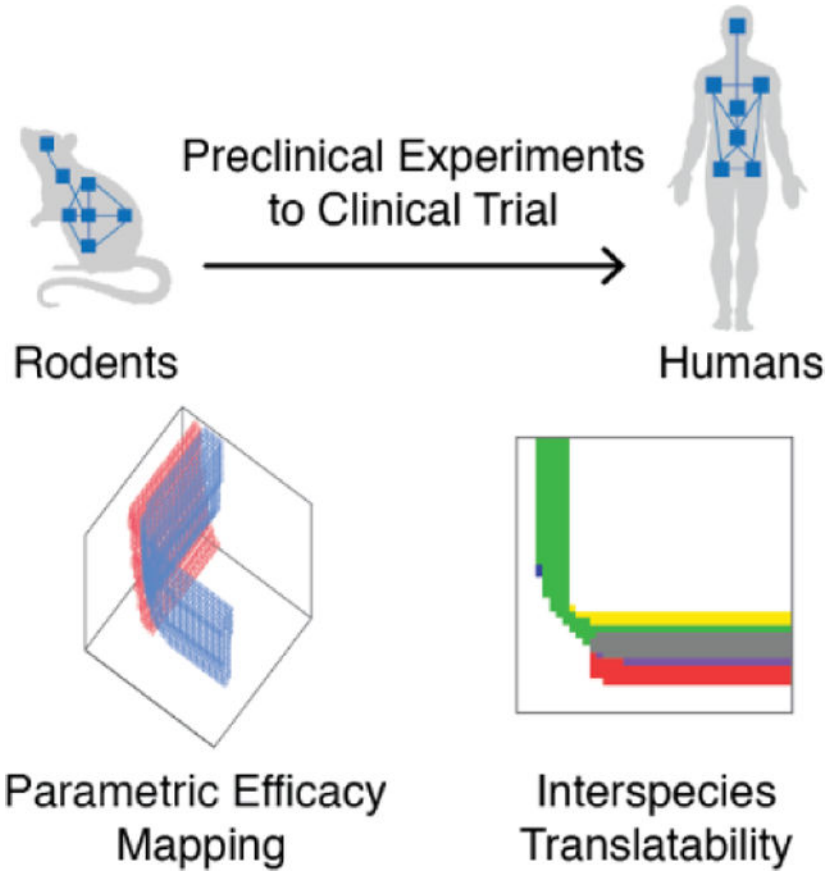

Keywords

glucose-responsive insulin; drug delivery; physiological modeling; diabetes

1. Introduction

Insulin is an endocrine hormone that regulates the plasma glucose level.[1] Exogenous insulin treatment is often subcutaneously administered for type 1 diabetes and advanced type 2 diabetes patients to mitigate insulin deficiency or high insulin resistance. As a result, daily injections significantly affect the quality of life for these patient populations.[2,3] Furthermore, precise control of the insulin dosing is required to maintain the plasma glucose level in the euglycemic range, 70–180 mg/dL, according to American Diabetes Association (ADA).[4] Plasma glucose concentrations outside this range can result in significant mortality and morbidity, making appropriate therapeutic administration paramount.

Plasma glucose level measurements are the most widely used method to diagnose and monitor diabetes. Continuous glucose monitoring technologies (CGM) allow for real-time glucose level monitoring, combined with closed-loop insulin administration, significantly removing patient-to-patient variability.[5,6] As CGM collects patients' daily plasma glucose profiles, several metrics were developed for better clinical care of diabetes patients. Time in range (TIR) of the euglycemic range, 70 – 180 mg/dL, has been introduced as an important metric to monitor the patients' glycemic management.[7] However, even with these state-of-the-art systems, the targeted TIR is 70 percent, meaning that the patients face the risk of hyper- or hypo-glycemia during 30 percent of their daily life.[8] Therefore, the concept of glucose-responsive insulin (GRI) and insulin delivery systems has been proposed and investigated to overcome the potential risk of hypoglycemia from insulin therapeutics.[9,10] GRI is an alternative insulin therapeutic designed to confront hypoglycemia: when the glucose level is high, the GRI performs similarly to native insulin, and when the glucose level is low, the GRI becomes deactivated. Therefore, accounting for the TIR assessment, GRI is expected to reduce the time under range.[11]

Since the GRI concept was first proposed in 1979[12], various strategies and mechanisms have been investigated. From insulin-containing polymeric particles to intrinsically modified insulin molecules, GRIs have been examined and proven to be successful in streptozotocin (STZ) induced diabetic animal models, including rodents[13–27], porcine[24,28], and canine[28]. However, only one subsequent unsuccessful human clinical evaluation was performed, a therapeutic named MK-2640.[28,29] Thus, the translation of GRI performance between animal experiments to human clinical trials is yet to be realized.

We have previously developed a computational model that can address questions quantitatively for the human or rodent (mouse or rat) endocrine systems, linking them using a common pharmacokinetic modeling framework.[30–32] Based on a whole-body compartmental model, we are able to simulate the endocrine system and glucoregulatory responses of humans, mice, and rats, with or without diabetes, and make predictions across species. In this work, we first classify GRI concepts demonstrated in the literature into three mechanistic classes: (1) intrinsic GRIs based on freely circulating insulin derivatives, (2) glucose-responsive particles that release insulin, and (3) glucose-responsive devices that inject insulin from a fixed location. We then generated numerical inputs for all three classes of GRI based on the simple kinetic representations. Next, using our computational model, PAMERAH, we simulated these GRIs with different mechanisms for each different organism. Based on ADA metrics for glucoregulation, we were able to determine optimal GRI designs. Subsequent comparisons between the design spaces of humans and model organisms highlight differences that would enable success in one and not the other. From this computational medicine approach, we assert that the time and cost associated with the development of GRI therapeutics and other technologies can be substantially reduced.

2. Classification of Glucose-responsive Insulin and Insulin Delivery Systems

To realize the GRI concept, researchers have proposed and investigated various approaches over several decades. In a recent review, Jarosinski et al. categorized GRI systems into mechanical systems, polymer-based GRI systems, and intrinsic GRI systems.[11] Wang et al. classified GRIs into three glucose-responsive moieties – glucose oxidase (GOx), phenylboronic acid (PBA), and glucose-binding molecules.[33] Shen et al. defined smart insulin delivery systems into four groups according to their sizes – glucose-responsive molecules and supramolecules, glucose-responsive particles, glucose-responsive macroscopic hydrogels, and glucose-responsive devices.[34] While acknowledging the merits and rationale for these previous classifications, this work necessarily has to group concepts by mechanistic action described as mathematical functions.

Herein, we adopt and modify the classification by Shen[34], using three mechanistic categories: (1) intrinsic GRI (iGRI), (2) glucose-responsive particles (GRPs), and (3) glucose-responsive insulin delivery devices (GRDs). We selected three representative cases for each category and modeled their therapeutic design spaces. Figure 1 summarizes the experimental examples and our proposed simplified GRI kinetics.

Class 1. Intrinsic GRI:

Intrinsic GRIs are insulin analogues with modified chemical moieties that modulate insulin efficacy based on the plasma glucose level. PBA and its derivatives are the most widely studied glucose sensor.[35,36] Glucose can reversibly bind with PBA moieties and changes the molecular structure of the insulin analogue. These structural changes of GRI impact the binding affinity of insulin analogue to the insulin receptor, and eventually, these insulin analogues exhibit glucose responsiveness. With this technique, Chen et al. developed fructose-responsive insulin and identified the mechanism of molecular modulation.[37] Alternatively, competitive binding of mannose receptors has also been adopted to control insulin efficacy. MK-2640 is an insulin saccharide conjugate that can bind the insulin receptor or mannose receptor C type 1, and it was the first clinically evaluated GRI analogue.[28,29]

For iGRI, we choose the reversible dormant insulin scheme[13], which has been shown in our previous work.[31,32] This scheme represents widely studied PBA-type intrinsic insulin analogues.[13,27] Innately inactive dormant GRIs can bind to glucose and acts like active insulin. The glucose binding reaction is modeled as reversible, and this dormant GRI circulates freely in the circulatory system. The kinetic equation of an iGRI is described below.

$$\text{Glucose (G)} + \text{Dormant insulin (D)} \underset{k_b}{\overset{k_f}{\rightleftharpoons}} \text{Insulin(I)}$$
$$\frac{d[I]}{dt} = k_f[G][D] - k_b[I] \quad \#(1)$$

Here, dormant GRI can reversibly bind to glucose and become active insulin. The forward (k_f) and backward (k_b) rate constants determine the glucose-responsive potency of GRI. The iGRIs were assumed freely circulating in the body, and the potency of iGRIs would be determined by local glucose concentration in each body compartment.

Class 2. Glucose-responsive Particles:

Glucose-responsive particles are micro- and nanoparticles loaded with insulin and glucose-responsive parts.[34] GRPs also circulate freely in the circulatory system, enabling triggered or delayed insulin delivery. Various strategies were explored to realize glucose-responsive particles. PBA and GOx are the most widely used glucose-responsive materials. As mentioned above, PBA offers reversible binding with glucose – but in this case, PBA is not attached to the insulin molecule but used as a polymeric structure that can deliver insulin. PBA-based polymer nanoparticles or membranes have been studied to develop a glucose-responsive insulin delivery system.[38–40]

The GOx enzyme is an alternative pathway to developing glucose responsiveness. GOx converts glucose into gluconic acid and hydrogen peroxide, and this reaction changes the local environment, especially the pH. The local pH change is sufficient to trigger pH-dependent polymer swelling or degradation, and by encapsulating insulin with these pH-responsive polymers, numerous GRPs have been developed.[18,19,41–44] Glucose oxidase-based particles utilize the reaction below.

$$\text{Glucose} + O_2 + H_2O \xrightarrow{GO_x} \text{Gluconic Acid} + H_2O_2 \quad \#(2)$$

For GRPs, GOx-based particles are chosen as a model system.[41] To model the insulin release behavior from these reservoirs, various mathematical models are available to describe drug release kinetics, including zeroth-order kinetics, first-order kinetics, the Higuchi model, and the Hixson-Crowell model.[45,46] In this case, we utilized the first-order kinetics to model the insulin release behavior of activated GRPs. The advantage of using the first-order kinetics is its ability to effectively map the therapeutic window of GRIs without sacrificing key physical properties. This kinetic scheme has been widely used in the literature to quantify drug release kinetics.[46,47] Similar to iGRI, we used the kinetic model with two parameters to effectively map the efficacy space. The kinetic equations of GRPs are described below.

$$\text{Glucose (G)} + \text{Inactive GRP (IG)} \xrightarrow{k_1} \text{Activated GRP(AG)} \xrightarrow{k_2} \text{Insulin } (I)$$
$$\frac{d[AG]}{dt} = k_1[G][IG] - k_2[AG] \quad \#(3)$$
$$\frac{d[I]}{dt} = k_2[AG]$$

Here, glucose reacts with inactive GRPs to activate the particles. This activated particle then starts to release insulin by degrading or swelling the insulin-containing matrix. Here, k_1 denotes activation rate constant, and k_2 denotes insulin releasing rate constant. Similar to the iGRI, GRPs are assumed to circulate freely in the body and share the insulin subsystem.

Notably, our model formulation inherently incorporates the lag in insulin release for GRPs and also GRDs. The insulin release rate constant, k_2, also functions as a lag in insulin release following glucose elevation. When k_2 has a larger value, the system exhibits fast diffusion, which minimizes the lag in insulin release. Conversely, a smaller k_2 value leads to a more prominent lag in insulin release, potentially impeding rapid regulation of the blood glucose levels.

Class 3. Glucose-responsive Devices:

Glucose-responsive insulin delivery devices are external devices that can be attached to the skin. These devices are millimeter-sized or larger.[34] Microneedle patches are the most common devices used for glucose-responsive delivery.[23,25,26,48,49] The insulin reservoir is connected to microneedles, which enables transdermal insulin delivery. Similar to GRPs, GOx and PBA are used for glucose sensing units. Additionally, mechanically driven glucose control systems, the so-called ‘artificial pancreas,’ can be considered glucose-responsive devices, but this system requires external electronics to monitor glucose levels and control insulin injection.[50]

For GRDs, we use similar kinetics to GRPs, but in this case, exogenous insulin is not freely circulating but fixed on the skin in the insulin reservoir, such as microneedle patches. The exogenous insulin is then delivered through the skin in response to muscle interstitial glucose concentration. The glucose responsiveness of GRDs originated from the composition of the microneedle. The kinetic equations of GRDs are described below.

$$\text{Glucose (G)} + \text{Inactive GRD} \xrightarrow{k_1} \text{Activated GRD (AG)} \xrightarrow{k_2} \text{Insulin}(I)$$
$$\frac{d[AG]}{dt} = k_1[G] - k_2[AG] \quad \#(4)$$
$$\frac{d[I]}{dt} = k_2[AG]$$

Glucose near the microneedle first reacts with GOx in the inactive GRDs. Similar to GRPs, these inactive GRDs are then activated and start to release insulin by degrading or swelling the insulin-containing matrix. Here again, k_1 denotes activation rate constant, and k_2 denotes the insulin releasing rate constant. We assumed the activation of the device is only dependent

on the local glucose concentration, as the glucose-responsive site (e.g., GOx) of the device is limited. For GRDs, the insulin is released to the muscle interstitial compartment, to which the transdermal patches are attached.

Additionally, recent advances in injectable hydrogel networks have demonstrated promising results in achieving glucose-responsive insulin delivery.[51–58] These injectable hydrogel networks are primarily administered via subcutaneous injection and are retained within the interstitial adipose space. Due to their injection site localization and lack of free circulation, they are classified as an example of the GRD system.

3. Model Construct / Formulation

3.1. Physiological Compartment Model

PAMERAH is a whole-body compartmental model to describe humans' and rodents' glucoregulatory systems. Built upon the previously introduced Sorensen model[59], PAMERAH can simulate three representative model systems: healthy and diabetic male humans with a body weight of 70 kg,[31] healthy or streptozotocin-induced (STZ) diabetic male Lewis rats with a body weight of 300 g, and healthy or STZ-induced diabetic male C57BL/6J mice with a body weight of 25 g.[32]

Figure 2a and 2b are schematics of our physiological model. Our model compartmentalized the body of humans and rodents into brain, heart and lung, liver, gut, muscle, and adipose, dividing each compartment into vascular and interstitial parts. All compartments are modeled as ideal well-mixed continuous stirred-tank reactors (CSTRs). Blood circulates through vascular compartments and transports glucose, insulin, glucagon, and GRI. In the interstitial compartment, nutrients and proteins diffuse in and out from vascular counterparts by the concentration gradients. The overall governing equations of the model are as follows:

$$V^{s}_{k,v}\frac{dC_{k,v}}{dt} = Q^{s}_{k,in}C_{k,v,in} - Q^{s}_{k,v}C_{k,v} - \frac{V^{s}_{k}}{T^{s}_{k}}(C_{k,v} - C_{k,i}) + R^{s}_{k,v,prod} - R^{s}_{k,v,cons} + V^{I}_{k,v}\nu_{s}r_{GRI} \quad \#(5)$$

$$V^{s}_{k,i}\frac{dC_{k,i}}{dt} = \frac{V^{s}_{k}}{T^{s}_{k}}(C_{k,v} - C_{k,i}) + R^{s}_{k,i,prod} - R^{s}_{k,i,cons} + V^{I}_{k,i}\nu_{s}r_{GRI} \quad \#\#(6)$$

where subscript k denotes organ compartment (e.g., brain, liver, kidney, etc.), subscripts v and i denote the vascular and interstitial compartment, respectively, and superscript **s** denotes the solutes: insulin (I), glucose (G), glucagon, and GRI. V is the volume of the compartment, C is the concentration of the solute in the compartment, $Q_{k,in}$ and $Q_{k,v}$ are the inlet and outlet flowrate to the compartment k, respectively, T is the transcapillary mass transfer time, and R_{prod} and R_{cons} are production or consumption rates of the solute in that compartment, respectively. r_{GRI} is the reaction rate for the GRI kinetics, and ν_s is the stoichiometric coefficient, which is −1, 1, 0, and −1 for insulin, glucose, glucagon, and GRI, respectively. Note that the GRI term in the equation is modular, which enables PAMERAH to simulate the glucoregulatory system with and without GRI. In addition,

PAMERAH is capable of simulating meal and feeding scenarios by incorporating an oral glucose absorption model.[30,31]

Our previous work demonstrated that PAMERAH could simulate a glucoregulatory system, including the glucose trajectory after insulin injection, meal consumption, and clamping studies. Figure 2c, 2d, and S1 show the plasma glucose trajectory of healthy and type 1 diabetic humans, rats, and mice after subcutaneous injection of insulin. Based on the Sorenson model, the pharmacokinetic model of humans was developed by Bakh et al.[31], and extended to rodents by Yang et al. [32] Figure 2c and 2d illustrate the plasma glucose trajectory of healthy and type 1 diabetic human, respectively, after subcutaneous injection of insulin dosing 1, 3, and 5 U. Detailed physiological and pharmacokinetic parameters for humans, rats and mice can be found in our previous publications.[31,32]

3.2 Time in range (TIR) Analysis for GRI Therapeutic Efficacy Evaluation

TIR is the amount of time that patients spend in the euglycemic range, normally between 70 and 180 mg/dL. TIR provides a numerical metric of how tight plasma glucose level was controlled over a given time interval. Compared to the hemoglobin A1c (HbA1c) metric that evaluates glycemic control over months, TIR is commonly used for cases needing high temporal resolution.[7,8]

As GRI is mainly designed to overcome the hypoglycemic risk from insulin therapeutics, we adopted the TIR framework to evaluate GRI efficacies. We adapted the TIR metric further to account for out-of-range plasma glucose levels through two risk scores. To account for the hyperglycemic risk of the therapeutics, we used the area above range 2 hours after the initial administration of insulin or GRI. For hypoglycemic risk, we use the area under range metric to determine how prolonged and severe the patients experience hypoglycemia.

$$\text{Hyperglycemic Risk Score } Z_{\text{hyper}} = \int_{2\text{h}}^{24\text{h}} \max\{(C_{g,plasma} - C_{g,ub}), 0\}\text{dt} \quad \#(7)$$

$$\text{Hypoglycemic Risk Score } Z_{\text{hypo}} = \int_{0\text{h}}^{24\text{h}} \max\ \{(C_{g,\text{lb}} - C_{g,\text{plasma}}), 0\}\text{dt} \quad \#(8)$$

Euglycemic range varies between human and model animals – here we used the plasma glucose level of humans, rats, and mice for 72 to 140 mg/dL [31,60], 63 to 200 mg/dL[32,61], 37 to 230 mg/dL[32,62], respectively, as euglycemic criteria. In TIR criteria, 70 to 180 mg/dL is typically used, but here, we selected a tighter range for human as an acceptable plasma glucose level after administering insulin and GRI. The efficacy of GRI is evaluated based on a one-day timeframe (24 hours), and meal or feeding scenarios are excluded in order to maintain an equal comparison across species.

4. Results and Discussion

4.1 Model-aided Design for Different Classes of GRI

Based on the GRI kinetics and physiological model described above, we simulated the glucose trajectory of any hypothetical GRI designed from one of the three classes described above. From obtained glucose trajectory, hypo- and hyperglycemia scores ($\mathbf{Z}_{\mathbf{hypo}}$ and $\mathbf{Z}_{\mathbf{hyper}}$) were calculated for TIR analysis. From this framework, we were able to map the optimal design space for each class of GRI.

Figure 3 illustrates the simulation results of class 1 intrinsic GRI, or iGRI. We investigated parameter space sized in a 41×41×33 grid, with forward (k_f) and backward (k_b) rate constants and dose per weight. The parameter space was chosen to maximize the overall optimal design regions. (ODRs) The forward and backward rate constant was investigated from 1.0×10^{-4} $M^{-1}min^{-1}$ to 1.0×10^{4} $M^{-1}min^{-1}$ and from 1.0×10^{-3} min^{-1} to 1.0×10^{5} min^{-1}, respectively. The ranges were chosen to maximize the region of optimal designs. The dosage of GRIs was chosen from 10 to 330 μg/kg for humans, rats, and mice.

Figure 3a to 3c represent what we label the GRI Design Space (GRIDS) for humans, rats, and mice, respectively. In the plots, each colored cube represents a viable GRI design parameter with zero hyper- and hypoglycemic risk scores defined in Equation 7 and 8. As can be seen in Figure 3, the percent of viable design space out of the entire parameter space were 4.08%, 5.18%, and 3.88%, for humans, rats, and mice, respectively.

In Figure 3d and 3e, overlaid GRIDS for humans and rats, and humans and mice are illustrated, respectively. A viable design region for interspecies translation can be obtained by overlaying obtained GRIDS for humans and rodents. The purple-colored region in Figure 3d and the green-colored region in Figure 3e indicate the overlapping viable parametric design space between humans and rats, and humans and mice, respectively.

Figure 3f shows a Venn Diagram of a therapeutic window of GRIs for humans, rats, and mice, which indicates the percentage of parametric space in the therapeutic range. The percent in the Venn Diagram is the percent of viable design space out of the entire parameter space (41×41×33 grid). Note that the overlap between rats and mice was much higher than that of humans.

The simulation results of class 2 glucose-responsive particles are shown in Figure 4. Similar to the iGRI simulation, we investigated the parameter space sized in a 41×41×33 grid, with the GRI activation reaction rate constant (k_1), insulin releasing rate constant (k_2) and dose per weight. Likewise, the parameter space was chosen to maximize the ODRs. The GRI activation reaction constant (k_1) and insulin releasing rate constant (k_2) were investigated from 1.0×10^{-3} $M^{-1}min^{-1}$ to 1.0×10^{5} $M^{-1}min^{-1}$ and from 1.0×10^{-4} min^{-1} to 1.0×10^{4} min^{-1}, respectively. The dosage of GRIs was chosen from 10 to 330 μg/kg for humans, rats, and mice.

Figure 4a to 4c represent the GRIDS for humans, rats, and mice, respectively. The percent of viable design space was 3.19%, 8.11%, and 8.41% for humans, rats, and mice, respectively.

Similar to Figure 3, Figure 4d and 4e illustrate the overlaid GRIDS for humans and rats, and humans and mice, respectively. Note that there was no overlap between humans and rodents. Figure 4f shows a Venn Diagram of the design space overlap of GRIs for humans, rats, and mice. Interestingly, rats and mice showed 6.88% design space overlap, while there was no overlap between humans and rodents.

Figure 5 illustrates the simulation results of class 3 glucose-responsive insulin delivery devices. For class 3, we investigated the parameter space sized in a 41×41×45 grid, with GRI activation reaction rate constant (k_1), insulin releasing rate constant (k_2) and dose per weight. The GRI activation reaction constant (k_1) and insulin releasing rate constant (k_2) were investigated from 1.0×10^{-3} $M^{-1}s^{-1}$ to 1.0×10^{5} $M^{-1}s^{-1}$ and from 1.0×10^{-4} s^{-1} to 1.0×10^{4} s^{-1}, respectively. The dosage of GRIs was chosen from 10 to 450 μg/kg for humans, rats, and mice. We increased the dosing range of class 3 compared to class 1 and 2, as the exogenous insulin is not freely circulating but fixed in the transdermal insulin reservoir. Similar to the previous analysis, Figure 5a to 5c represent the GRIDS for humans, rats, and mice. The percent of viable design space was 8.56%, 3.04%, and 7.57% for humans, rats, and mice, respectively. Figure 5d and 5e illustrate the overlaid GRIDS for humans and rats, and humans and mice. Similar to GRPs, there was no overlap between humans and rodents. Figure 5f shows a Venn Diagram of the design space overlap of GRIs for humans, rats, and mice. Notably, the GRIDS of rats is a subset of the GRIDS of mice, while there was no overlap of GRIDS between humans and rodents.

4.2 Interspecies Translatability Analysis of GRI

The ultimate goal of the GRI is to become medically relevant therapeutics for diabetic patients to achieve better glycemic control and improve quality of life. However, currently reported GRIs mostly remain in the pre-clinical stage supported by *in vivo* animal experiments, and only one GRI that has moved on to human clinical evaluation was unsuccessful.[29] Thus, translating pre-clinical promise to clinical success is the most crucial aspect of developing therapeutics.

Our mathematical model PAMERAH is designed to map the efficacy space of a GRI in humans for comparison to performance in rodents, reflecting the use of animal models in the research and development process. With this computational framework, we performed an interspecies translatability analysis on each GRI class. Here, we define interspecies translatability as the probability of clinical success of the therapeutics from the successful preclinical rodent experiments. In Figure 3, 4, and 5, we illustrate the effective design space that can maintain the glycemic level for humans, rats, and mice. From the 3-axis parametric design space of dose and kinetic parameters, we are able to provide the 3D overlapping region ideal for clinical translation. The colored volume in overlaid GRIDS indicates the optimal design region that might be both effective in humans and rodents. Surprisingly, we observed an overlapping region between humans and rodents only in Class 1 iGRI. In contrast, for Class 2 GRPs and Class 3 GRDs, we predict that the ODRs for humans and rodents do not overlap. This has negative implications for the utility of pre-clinical testing on mice or rat models for GRPs and GRDs. However, our results suggest that mice and rat testing for iGRIs can inform human efficacy.

Considering the difficulties of synthetically tuning the parameters of each GRI, we note that they are significantly more challenging to change compared to the administered dosage of the GRI. With that regard, we lumped the z-axis in the previous GRIDS analysis and mapped the efficacy space based on the kinetic parameters of each GRI. Figure 6a to 6c illustrates the projected design space for each type of GRI. With this 2D parametric space, we are able to observe overlapped regions between humans and rodents in all three GRI classes. Based on this mapping, we evaluated the probability of successful translation between humans and rodents in Figure 6d. The true positive is defined as the area overlapping with both humans and rodents divided by the area of rodents. The false positive is defined as the area only for rodents divided by the whole area of rodents.

$$\text{True Positive} = \frac{A_{\text{human}} \cap A_{\text{rodent}}}{A_{\text{rodent}}} \quad \#(9)$$

$$\text{False Positive} = 1 - \frac{A_{\text{human}} \cap A_{\text{rodent}}}{A_{\text{rodent}}} \quad \#(10)$$

The probability of true positive between rats and humans is 67.3 %, 46.1 %, and 28.1 % for iGRIs, GRPs, and GRDs, respectively. The probability of true positive between mice and humans is 50.5 %, 33.9 %, and 30.9 % for iGRIs, GRPs, and GRDS, respectively, which are slightly lower than for rats in iGRIs and GRPs. The probability of false positive between rats and humans is 32.7 %, 53.9 %, and 71.9 % for iGRIs, GRPs, and GRDs, respectively, and the probability of false positive between mice and humans is 49.5 %, 66.1 %, and 69.1 % for iGRIs, GRPs, and GRDs, respectively. From this analysis, we observed that the iGRI system has the highest probability of successful translation, and GRDs have the lowest probability of successful translation among the three classes, assuming the same level of synthetic control over the parameters associated with each.

5. Outlooks and Conclusion

In this work, we classified and evaluated the potential translatability of GRIs based on their computed efficacies in different model organisms. We first categorized existing GRI candidates into three distinct mechanistic classes: (1) intrinsic GRIs, (2) glucose-responsive particles, and (3) glucose-responsive devices. We argued that this classification will be helpful for comparing GRI results in the literature. We then created models of these GRI kinetics and introduced them to our whole-body compartment physiological model. Using this system, we simulated the effect of GRI action and map the design space for each GRI class for humans and rodents based on time in range metric. Furthermore, by comparing the design space overlap for parameters that satisfy desired metrics, we evaluated the translatability of each GRI class between rodents and humans. From our analysis, iGRIs had the highest true positive, a metric for interspecies overlap, which indicated the most probable clinical translation success, followed by GRPs and GRDs. However, our analysis was based on the simplest kinetic model to capture the chemistry of each GRI class. By integrating multiple components such as: a robust kinetic model, *in vitro* assay, and *in vivo*

animal experiment data, our model would provide better mechanistic understandings and improved predictions of clinical translatability.

5.1 Comparative Analysis of GRI Systems – Toward Successful Clinical GRI Therapeutics

In Figures 3 to 6, we explored the ODRs in parametric design space for each GRI class. In our 3D GRIDS analysis, we noticed that the ODRs for humans and rodents do not overlap in GRPs and GRDs, which implied that the translation between humans and rodents is relatively more difficult compared to iGRIs. In Figure 6, assuming equal difficulty in tuning kinetic parameters across the three classes, we observed that the probability of successful translation is the highest in iGRIs, followed by GRPs and GRDs. From this analysis, it might be more difficult to achieve successful clinical translation for GRDs compared to iGRIs. A caveat with this assertion, however, is that it is not equally challenging to modify activation kinetics for these classes, which depends on state-of-the-art synthetic capabilities.

Expanding on this point further, our analysis only accounted for the intrinsic kinetic properties of model GRIs. Considering the difficulties of tuning the intrinsic properties of different GRIs, it can be argued that GRPs and GRDs are more easily tunable in terms of size, shape, porosity, and other physical parameters compared to iGRIs. The strategy employed by iGRI to achieve glucose responsiveness involves covalent functionalization of insulin with additional chemical and biological components. This implies that the binding affinity of GRI to glucose is governed solely by the intrinsic properties of molecular design. In contrast, for the GRPs and GRDs, insulin is not chemically modified but rather transported by nano- or microparticle carriers or macroscopic devices. The design aspects of GRPs and GRDs are relatively more tunable than the modification of the chemical and biological properties in iGRIs, leading to more extensive research on GRPs and GRDs as opposed to iGRIs.

In case of GRPs, factors such as particle size, insulin loading, or GOx loading determines the insulin-releasing dynamics. Successful GRPs can be achieved by modifying particle size and synthesis stoichiometries without altering the fundamental chemistry of the particles. Likewise, the GRDs seem to have more routes to adjust their insulin release kinetics by optimizing the device design, such as the density of the microneedle per area, the size of the microneedle patch, or even the length of the microneedle. With these considerations, GRPs and GRDs may be able to address the challenges with limited translatability by engineering their physical properties.

As mentioned in section 3.1, the physiological model is based on three representative cases: 70 kg adult male human, 300 g male Lewis rat, and 25 g male C57BL/6J mouse. The model did not include individual variations such as weight, sex, or age in this study. This individual variance might deteriorate the final translatability of the designed GRI based on the model.

In addition, in the absence of information to the contrary, we assumed that the activated GRIs or released exogenous insulin acts exactly the same as regular human insulin. However, modifying insulin molecules in iGRIs might lower the activity of insulin analogues by lowering the binding affinity to insulin receptors. This deviation can be quantitatively adjusted in the model from experiments, especially glucose clamping studies.

PAMERAH can perform clamping simulation as well, and by comparing and fitting the simulation and experiments, we can capture the experimental properties of designed GRIs.

Finally, in this work, we utilized irreversible, ideal elementary reaction kinetics to model the activation of GRI and first-order kinetics to describe the subsequent insulin release in GRPs and GRDs. Nonetheless, in actual experimental conditions, more complex kinetics may be encountered, including undesirable insulin leakage, glucose cooperativity, or reversible glucose-binding kinetics. In future work, these nonlinear, complex kinetics will be incorporated into the analysis for specific GRI therapeutics, as elaborated in Supplementary Note 1.1.

5.2 A Priori Model-aided Design and A Posteriori Investigation of GRIs

The advances in biotechnology enable new form factors of therapeutics through protein engineering, synthesis of nanoparticle carriers, and exogenous device for long-term drug delivery. In this work, we demonstrated that PAMERAH is capable of simulating the pharmacokinetics of different classes of GRI with different sizes and form factors. We envision PAMERAH to boost GRI development in two ways: by providing *a priori* design constraints in the screening stage and by extracting physical and chemical parameters *a posteriori* from the experiments.

In this work, we used the simplest kinetics to explain GRI dynamics for providing general ODR maps in each class. For example, we used the GRI activation reaction rate constant (k_1), insulin releasing rate constant (k_2) to seek optimal design space for Class 2 GRPs and Class 3 GRDs. From our ODR mapping analysis, we are able to quantify the viable ranges of kinetic constants with respect to their scale, order of magnitude, and the relative difference between the two parameters. In addition, these kinetic constants can be translated into physical variables. For instance, the GRI activation rate constant is directly correlated to the glucose oxidation reaction by GOx. Insulin releasing rate constant is related to the diffusivity of insulin from the polymer matrix or geometry of the GRDs. For more practical use of PAMERAH, the user can define more complex and explanatory kinetics for the specific design. By providing more complex kinetics to the model, PAMERAH can generate more precise ODR maps that might resemble the real physics of the selected GRI scheme. Additionally, meals and feeding condition can be integrated into the model for simulating real-world scenarios, particularly when transitioning novel GRI therapeutics to the clinical stages.

In addition to ODR mapping, PAMERAH offers its own merit for allometric scaling and safe dose prediction for clinical trials. In this work, we used dose per weight to compare the equivalent dose for humans and rodents. However, body surface area is another important allometric scale for translation,[63] and our model is capable of comparing the efficacy with dose per body surface area, by rescaling the dose axes. (Figure S2) Moreover, it is recommended to utilize physiological, pharmacokinetic, and toxicology data for interspecies scaling.[64] Our model can predict the equivalent dose for interspecies scaling by incorporating the *in vitro* experiment data and performing clamping simulations. Given that our model is based on fundamental physiology and pharmacokinetics of glucoregulatory

systems, we anticipate it will provide a more accurate estimate of therapeutic dose for clinical trials.

Also, PAMERAH is advantageous for extracting the kinetic parameters. Currently, the kinetic parameters of GRIs are mainly studied with *in vitro* assays to find the binding affinities of GRI to insulin receptors for iGRIs. For GRPs, glucose responsiveness is tested by measuring insulin release in certain glucose concentrations. However, these *in vitro* results do not guarantee the success *in vivo* animal experiments, as the conditions in the confined circulatory system and animal body differ from *in vitro* experimental conditions. With PAMERAH, the user can extract the *in vivo* kinetics of the GRI by fitting the experimental glucose trajectory in the model. Thus, we envision that this computational medicine framework could contribute to accelerating GRI development. It is noteworthy that PAMERAH and models like it may reduce the reliance on animal testing for clinical translation, or reduce the requite size of the animal study, further aiding the development and testing pipeline.

Supplementary Material

Refer to Web version on PubMed Central for supplementary material.

Acknowledgements

The authors would like to acknowledge NIH grant number 1R01DK127761 to Weiss at IU for insight into class 1 GRIs (iGRIs). We also acknowledge a grant from the Helmsley foundation to Strano at MIT, No. 2202-05781, for support of PAMERAH development and refinement.

This study probes the therapeutic efficacies and potential clinical translatability of existing glucose-responsive insulins (GRIs) and insulin delivery systems, using a pharmacokinetic model to simulate the glucoregulatory system of humans and rodents. This computational framework can be used to predict the efficacy and translatability, which can contribute to accelerating GRI development.

References

[1]. Petersen MC, Shulman GI, Physiol Rev 2018, 98, 2133. [PubMed: 30067154]

[2]. Rubin RR, Peyrot M, Diabetes Metab Res Rev 1999, 15, 205. [PubMed: 10441043]

[3]. Laffel LMB, Connell A, Vangsness L, Goebel-Fabbri A, Mansfield A, Anderson BJ, Diabetes Care 2003, 26, 3067. [PubMed: 14578241]

[4]. Care D, Suppl SS, Diabetes Care 2022, 45, S83. [PubMed: 34964868]

[5]. Ovalle F, Yearbook of Endocrinology 2009, 2009, 34.

[6]. Rodbard D, Diabetes Technol Ther 2016, 18, S2. [PubMed: 26836425]

[7]. Beck RW, Bergenstal RM, Riddlesworth TD, Kollman C, Li Z, Brown AS, Close KL, Diabetes Care 2019, 42, 400. [PubMed: 30352896]

[8]. Battelino T, Danne T, Bergenstal RM, Amiel SA, Beck R, Biester T, Bosi E, Buckingham BA, Cefalu WT, Close KL, et al., Diabetes Care 2019, 42, 1593. [PubMed: 31177185]

[9]. Zaykov AN, Mayer JP, DiMarchi RD, Nat Rev Drug Discov 2016, 15, 425. [PubMed: 26988411]

[10]. Bakh NA, Cortinas AB, Weiss MA, Langer RS, Anderson DG, Gu Z, Dutta S, Strano MS, Nat Chem 2017, 9, 937. [PubMed: 28937662]

[11]. Jarosinski MA, Dhayalan B, Rege N, Chatterjee D, Weiss MA, Diabetologia 2021, 64, 1016. [PubMed: 33710398]

[12]. Brownlee M, Cerami A, Science (1979) 1979, 206, 1190.

[13]. Chou DH-C, Webber MJ, Tang BC, Lin AB, Thapa LS, Deng D, Truong JV, Cortinas AB, Langer R, Anderson DG, Proceedings of the National Academy of Sciences 2015, 112, 2401.

[14]. Wang J, Yu J, Zhang Y, Kahkoska AR, Wang Z, Fang J, Whitelegge JP, Li S, Buse JB, Gu Z, Proceedings of the National Academy of Sciences 2019, 116, 10744.

[15]. Mannerstedt K, Mishra NK, Engholm E, Lundh M, Madsen CS, Pedersen PJ, Le-Huu P, Pedersen SL, Buch-Månson N, Borgström B, et al., Chemistry – A European Journal 2021, 27, 3166. [PubMed: 33169429]

[16]. Yang R, Wu M, Lin S, Nargund RP, Li X, Kelly T, Yan L, Dai G, Qian Y, Dallas-yang Q, et al., JCI Insight 2018, 3, e97476. [PubMed: 29321379]

[17]. Li X, Fu M, Wu J, Zhang C, Deng X, Dhinakar A, Huang W, Qian H, Ge L, Acta Biomater 2017, 51, 294. [PubMed: 28069504]

[18]. Gu Z, Aimetti AA, Wang Q, Dang TT, Zhang Y, Veiseh O, Cheng H, Langer RS, Anderson DG, ACS Nano 2013, 7, 4194. [PubMed: 23638642]

[19]. Gu Z, Dang TT, Ma M, Tang BC, Cheng H, Jiang S, Dong Y, Zhang Y, Anderson DG, ACS Nano 2013, 7, 6758. [PubMed: 23834678]

[20]. Gordijo CR, Koulajian K, Shuhendler AJ, Bonifacio LD, Huang HY, Chiang S, Ozin GA, Giacca A, Wu XY, Adv Funct Mater 2011, 21, 73.

[21]. Chu MKL, Chen J, Gordijo CR, Chiang S, Ivovic A, Koulajian K, Giacca A, Wu XY, Sun Y, Lab Chip 2012, 12, 2533. [PubMed: 22565220]

[22]. Tai W, Mo R, Di J, Subramanian V, Gu X, Buse JB, Gu Z, Biomacromolecules 2014, 15, 3495. [PubMed: 25268758]

[23]. Xu B, Cao Q, Zhang Y, Yu W, Zhu J, Liu D, Jiang G, ACS Biomater Sci Eng 2018, 4, 2473. [PubMed: 33435111]

[24]. Wang J, Yu J, Zhang Y, Zhang X, Kahkoska AR, Chen G, Wang Z, Sun W, Cai L, Chen Z, et al., Sci Adv 2019, 5, 4357.

[25]. Hu X, Yu J, Qian C, Lu Y, Kahkoska AR, Xie Z, Jing X, Buse JB, Gu Z, ACS Nano 2017, 11, 613. [PubMed: 28051306]

[26]. Wang J, Ye Y, Yu J, Kahkoska AR, Zhang X, Wang C, Sun W, Corder RD, Chen Z, Khan SA, et al., ACS Nano 2018, 12, 2466. [PubMed: 29455516]

[27]. Qiu Y, Agrawal R, Chen D, Zheng N, Durupt G, Kim JH, Fisher SJ, Chou DHC, Adv Ther (Weinh) 2019, 2, DOI 10.1002/adtp.201900128.

[28]. Kaarsholm NC, Lin S, Yan L, Kelly T, Van Heek M, Mu J, Wu M, Dai G, Cui Y, Zhu Y, et al., Diabetes 2018, 67, 299. [PubMed: 29097375]

[29]. Krug AW, Visser SAG, Tsai K, Kandala B, Fancourt C, Thornton B, Morrow L, Kaarsholm NC, Bernstein HS, Stoch SA, et al., Clin Pharmacol Ther 2019, 105, 417. [PubMed: 30125349]

[30]. Bisker G, Iverson NM, Ahn J, Strano MS, Adv Healthc Mater 2015, 4, 87. [PubMed: 25080048]

[31]. Bakh NA, Bisker G, Lee MA, Gong X, Strano MS, Adv Healthc Mater 2017, 6, 1700601.

[32]. Yang JF, Gong X, Bakh NA, Carr K, Phillips NFB, Ismail-Beigi F, Weiss MA, Strano MS, Diabetes 2020, 69, 1815. [PubMed: 32152206]

[33]. Wang J, Wang Z, Yu J, Kahkoska AR, Buse JB, Gu Z, Advanced Materials 2020, 32, 1.

[34]. Shen D, Yu H, Wang L, Khan A, Haq F, Chen X, Huang Q, Teng L, Journal of Controlled Release 2020, 321, 236. [PubMed: 32061789]

[35]. Friedman S, Pizer R, J Am Chem Soc 1975, 97, 6059.

[36]. Wu X, Li Z, Chen X-X, Fossey JS, James TD, Jiang Y-B, Chem Soc Rev 2013, 42, 8032. [PubMed: 23860576]

[37]. Chen Y-S, Gleaton J, Yang Y, Dhayalan B, Phillips NB, Liu Y, Broadwater L, Jarosinski MA, Chatterjee D, Lawrence MC, et al., Proceedings of the National Academy of Sciences 2021, 118, 1.

[38]. Shi D, Ran M, Zhang L, Huang H, Li X, Chen M, Akashi M, ACS Appl Mater Interfaces 2016, 8, 13688. [PubMed: 27210795]

[39]. Wu J-Z, Williams GR, Li H-Y, Wang D-X, Li S-D, Zhu L-M, Drug Deliv 2017, 24, 1513. [PubMed: 28975813]

[40]. Yuan W, Shen T, Wang J, Zou H, Polym Chem 2014, 5, 3968.
[41]. Kim MY, Kim J, ACS Biomater Sci Eng 2017, 3, 572. [PubMed: 33429624]
[42]. Farahani BV, Ghasemzaheh H, Afraz S, RSC Adv 2016, 6, 26590.
[43]. Lim ZW, Ping Y, Miserez A, Bioconjug Chem 2018, 29, 2176. [PubMed: 29944344]
[44]. Chen W-H, Luo G-F, Vázquez-González M, Cazelles R, Sohn YS, Nechushtai R, Mandel Y, Willner I, ACS Nano 2018, 12, 7538. [PubMed: 29969227]
[45]. Siepmann J, Siepmann F, Int J Pharm 2008, 364, 328. [PubMed: 18822362]
[46]. Lassalle V, Ferreira ML, Journal of Chemical Technology & Biotechnology 2010, 85, 1588.
[47]. Yu S, Xian S, Ye Z, Pramudya I, Webber MJ, J Am Chem Soc 2021, 143, 12578. [PubMed: 34280305]
[48]. Yu J, Zhang Y, Ye Y, DiSanto R, Sun W, Ranson D, Ligler FS, Buse JB, Gu Z, Proceedings of the National Academy of Sciences 2015, 112, 8260.
[49]. Yu J, Wang J, Zhang Y, Chen G, Mao W, Ye Y, Kahkoska AR, Buse JB, Langer R, Gu Z, Nat Biomed Eng 2020, 4, 499. [PubMed: 32015407]
[50]. Haidar A, IEEE Control Syst 2016, 36, 28.
[51]. Li X, Fu M, Wu J, Zhang C, Deng X, Dhinakar A, Huang W, Qian H, Ge L, Acta Biomater 2017, 51, 294. [PubMed: 28069504]
[52]. Dong Y, Wang W, Veiseh O, Appel EA, Xue K, Webber MJ, Tang BC, Yang X-W, Weir GC, Langer R, et al., Langmuir 2016, 32, 8743. [PubMed: 27455412]
[53]. Zhao F, Wu D, Yao D, Guo R, Wang W, Dong A, Kong D, Zhang J, Acta Biomater 2017, 64, 334. [PubMed: 28974477]
[54]. Lu Y, Yu H, Wang L, Shen D, Liu J, ChemistrySelect 2021, 6, 11664.
[55]. Mandal D, Mandal SK, Ghosh M, Das PK, Chemistry - A European Journal 2015, 21, 12042. [PubMed: 26184777]
[56]. Yesilyurt V, Webber MJ, Appel EA, Godwin C, Langer R, Anderson DG, Advanced Materials 2016, 28, 86. [PubMed: 26540021]
[57]. Zhang M, Song C-C, Du F-S, Li Z-C, ACS Appl Mater Interfaces 2017, 9, 25905. [PubMed: 28714308]
[58]. Xian S, VandenBerg MA, Xiang Y, Yu S, Webber MJ, ACS Biomater Sci Eng 2022, 8, 4873. [PubMed: 36317822]
[59]. Sorensen JT, Ph.D. Thesis, MIT, Cambridge, MA, 1985.
[60]. Cryer PE, Davis SN, Shamoon H, Diabetes Care 2003, 26, 1902. [PubMed: 12766131]
[61]. Maheandiran M, Mylvaganam S, Wu C, El-Hayek Y, Sugumar S, Hazrati L, Del Campo M, Giacca A, Zhang L, Carlen PL, PLoS One 2013, 8, e83168. [PubMed: 24386156]
[62]. Grant CW, Duclos SK, Moran-Paul CM, Yahalom B, Tirabassi RS, Arreaza-Rubin G, Spain LM, Guberski DL, Comp Med 2012, 62, 381. [PubMed: 23114041]
[63]. Gouma E, Simos Y, Verginadis I, Lykoudis E, Evangelou A, Karkabounas S, Lab Anim 2012, 46, 40. [PubMed: 22008848]
[64]. Blanchard OL, Smoliga JM, The FASEB Journal 2015, 29, 1629. [PubMed: 25657112]

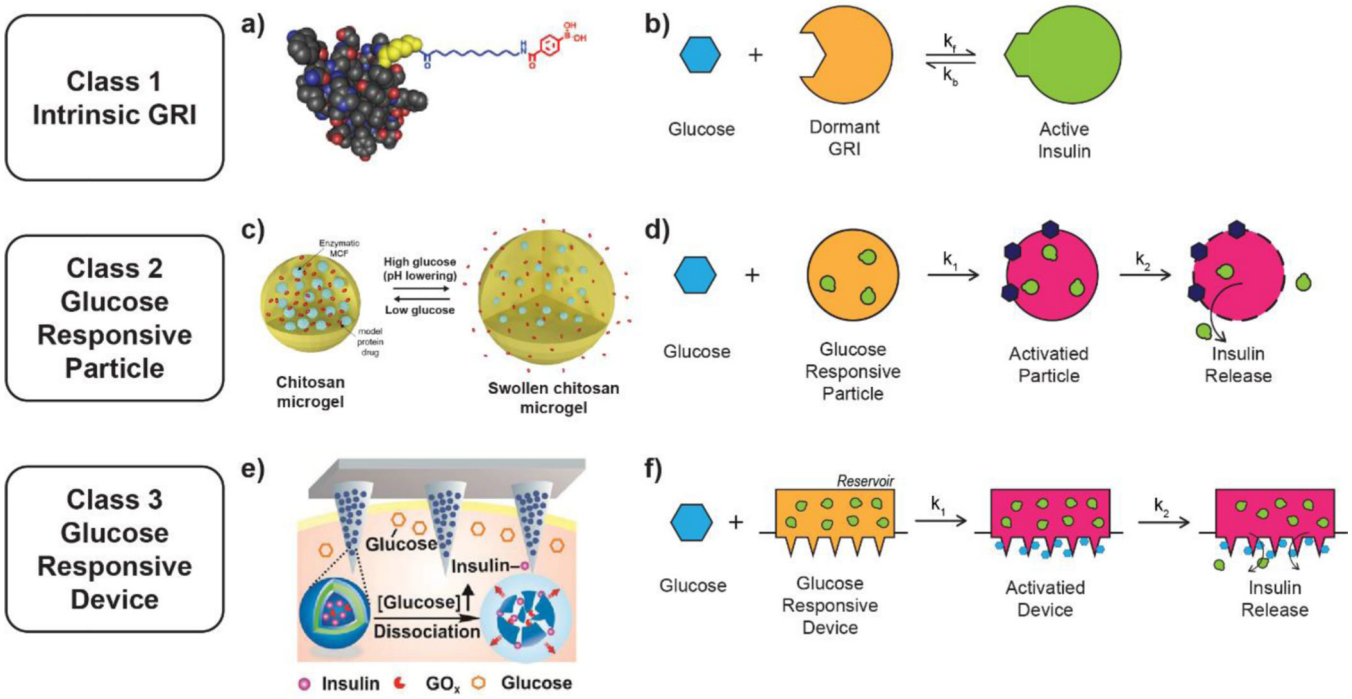

Figure 1.

Classification of glucose-responsive insulin and insulin delivery systems. a-b: Class 1 Intrinsic GRI (iGRI), c-d: Class 2 Glucose-responsive particle (GRP), e-f: Class 3 Glucose-responsive device (GRD). a) An example iGRI: PBA-modified long-acting insulin derivative. Reproduced with permission.[13] Copyright 2015, the National Academy of Sciences of the United States of America. b) Schematics of kinetic mechanism for iGRI. c) An example GRP: Nanoparticles that encapsulate insulin and glucose-specific enzymes. Reproduced with permission.[41] Copyright 2017, ACS. d) Schematics of kinetic mechanism for GRP. e) An example GRD: Glucose-responsive microneedle patch for insulin delivery. Reproduced with permission.[25] Copyright 2017, ACS. f) Schematics of kinetic mechanism for GRD.

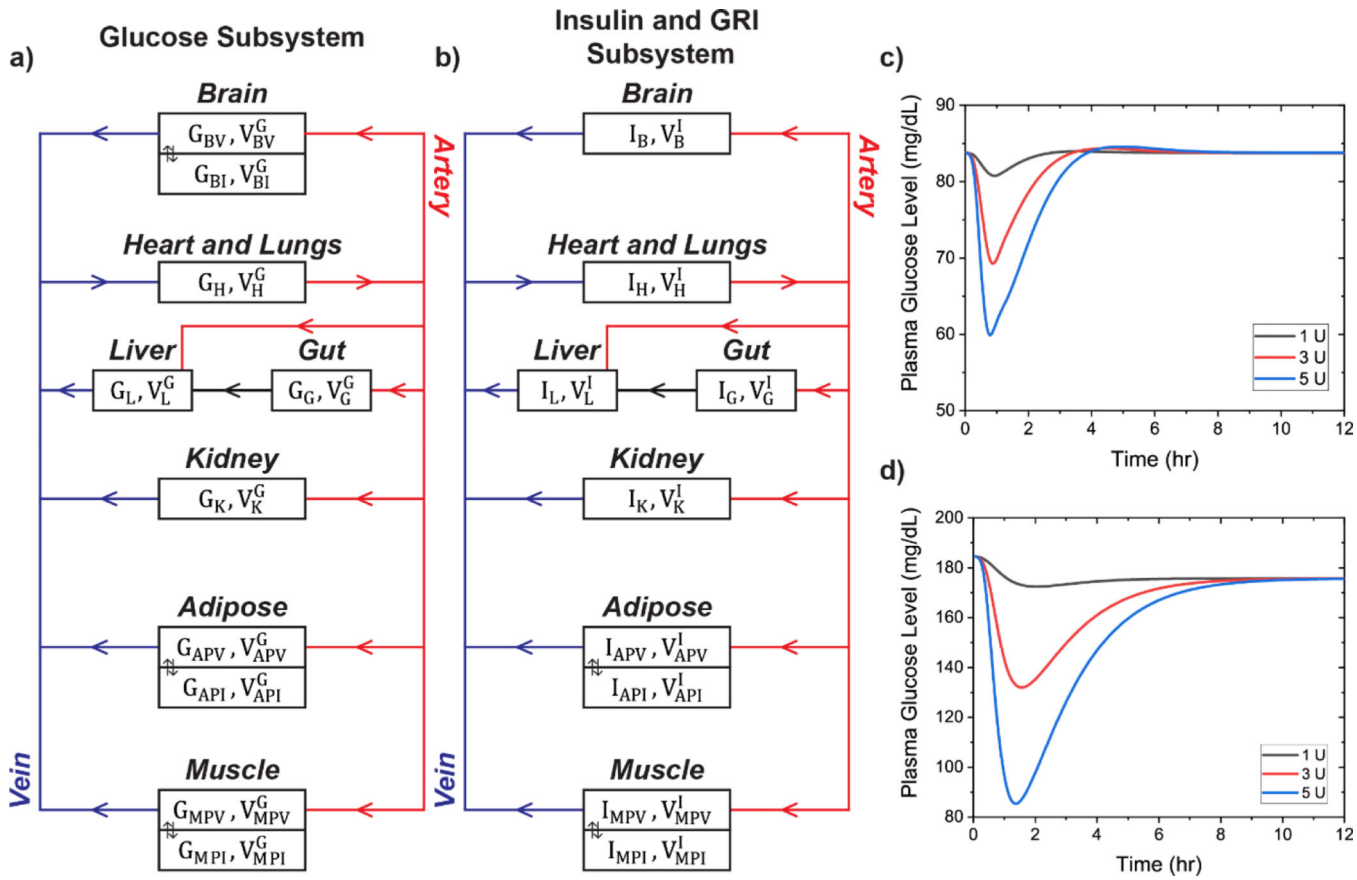

Figure 2.

Schematics of the PAMERAH compartmental model structure and plasma glucose profile after subcutaneous injection of regular human insulin. a) Schematics of glucose sub-model and b) insulin or GRI sub-model. Our model compartmentalized the body of humans and rodents into brain, heart and lung, liver, gut, muscle, and adipose, assuming all compartments as ideal well-mixed continuous stirred-tank reactors. c) Plasma glucose profile of healthy and d) diabetic human after subcutaneous dosing of 1 U, 3 U, and 5 U insulin. By solving the system of ordinary differential equations (Equation 5 and 6), we are able to predict time course of glucose and insulin concentrations in each compartment.

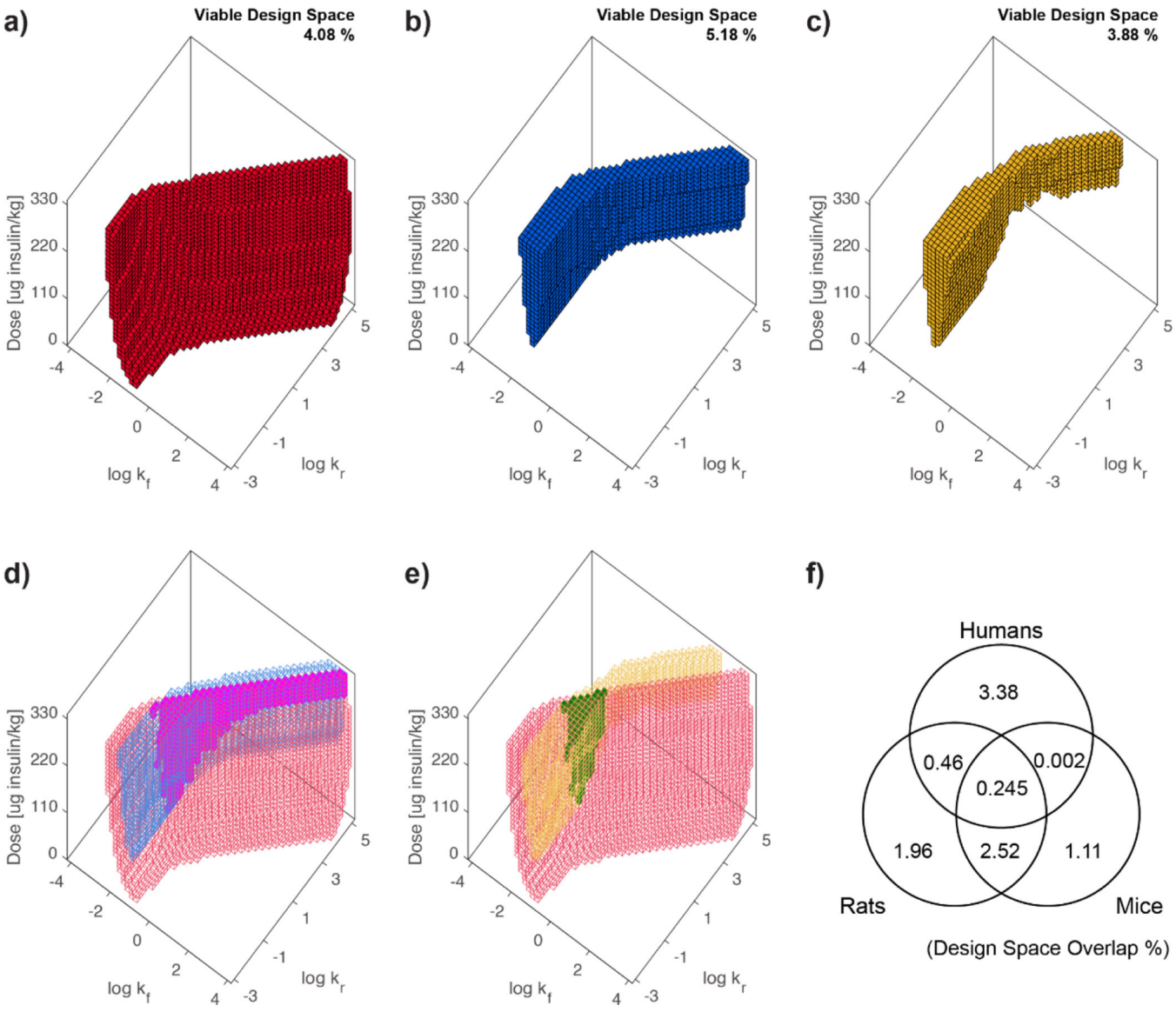

Figure 3.

Parametric GRI efficacy mapping results of Class 1 intrinsic GRI (iGRI) for a) humans, b) rats, and c) mice. Forward (k_f) and backward (k_b) rate constants of iGRI and dose per weight are chosen as parametric design space. The colored regions of the plot indicates that both hypoglycemic and hyperglycemic risk scores (Equation 7 and 8) are zero, displaying therapeutics that are efficacious. d) Overlaid GRIDS between humans and rats. Purple-colored region are the overlapping volume between the two organisms, which indicates potentially successfully navigating clinical trials. e) Overlaid GRIDS between humans and mice. Green-colored region are the overlapping volume, which indicates potentially successful clinical translation. f) Venn Diagram that summarizes the viable design space for humans and rodents, where the numerical values represent the percent volume of the viable regions for each cube. The intersection shows interspecies design space overlap, indicating that the therapeutics would be efficacious for both species.

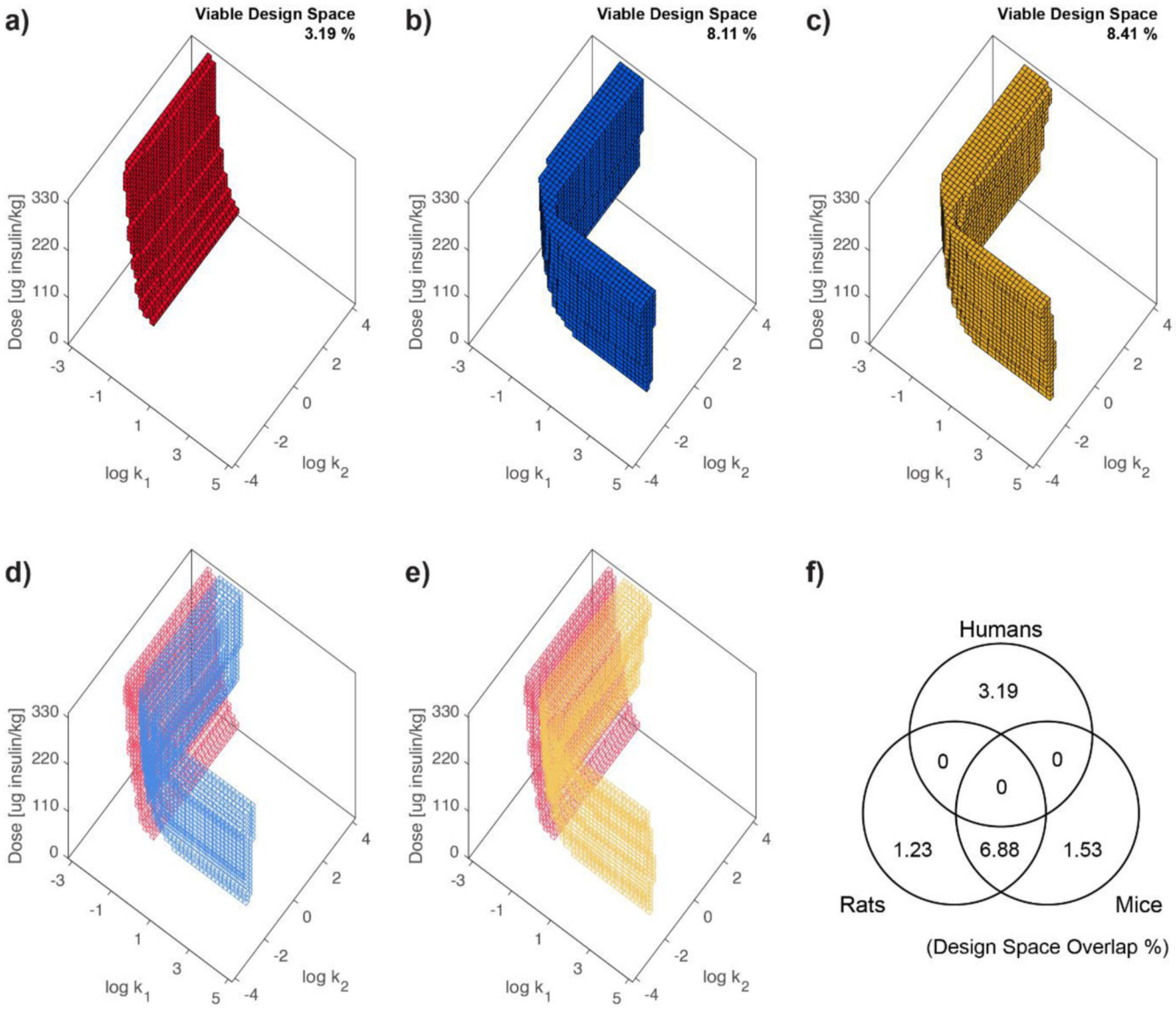

Figure 4.

Parametric GRI efficacy mapping results of Class 2 Glucose-Responsive Particles (GRP) for a) humans, b) rats, and c) mice. GRI activation reaction constant (k_1), insulin releasing rate constant (k_2) of GRP and dose per weight are chosen as parametric design space. d) Overlaid GRIDS between humans and rats, and e) overlaid GRIDS between humans and mice. f) Venn Diagram of viable design space for humans and rodents. The intersection shows interspecies design space overlap, indicating that the therapeutics would be efficacious for both species.

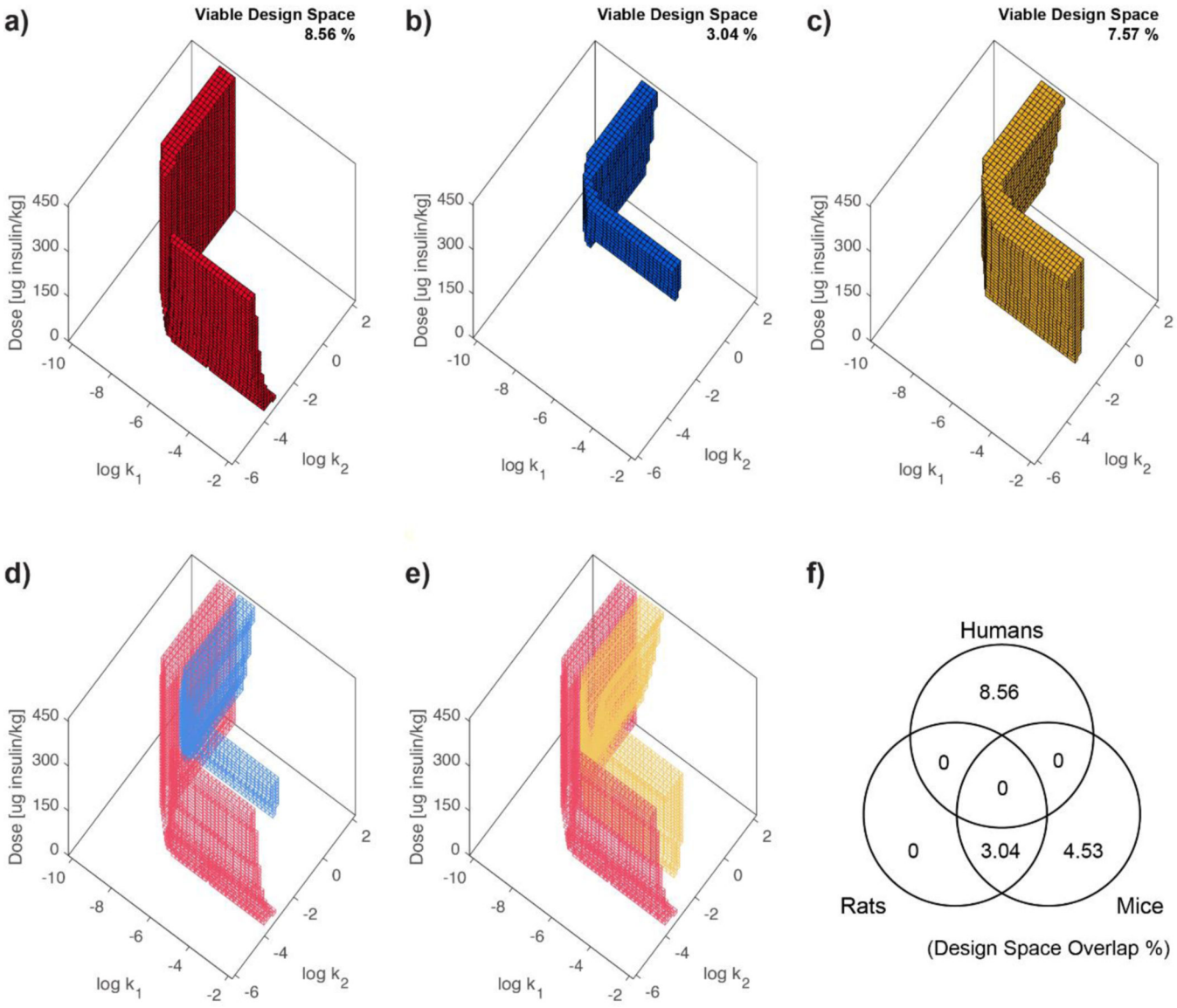

Figure 5.

Parametric GRI efficacy mapping results of Class 3 glucose-responsive insulin delivery devices (GRD) for a) humans, b) rats, and c) mice. GRI activation reaction constant (k_1), insulin releasing rate constant (k_2) of GRP and dose per weight are chosen as parametric design space. d) Overlaid GRIDS between humans and rats, and e) overlaid GRIDS between humans and mice. f) Venn Diagram of viable design space for humans and rodents. The intersection shows interspecies design space overlap, indicating that the therapeutics would be efficacious for both species.

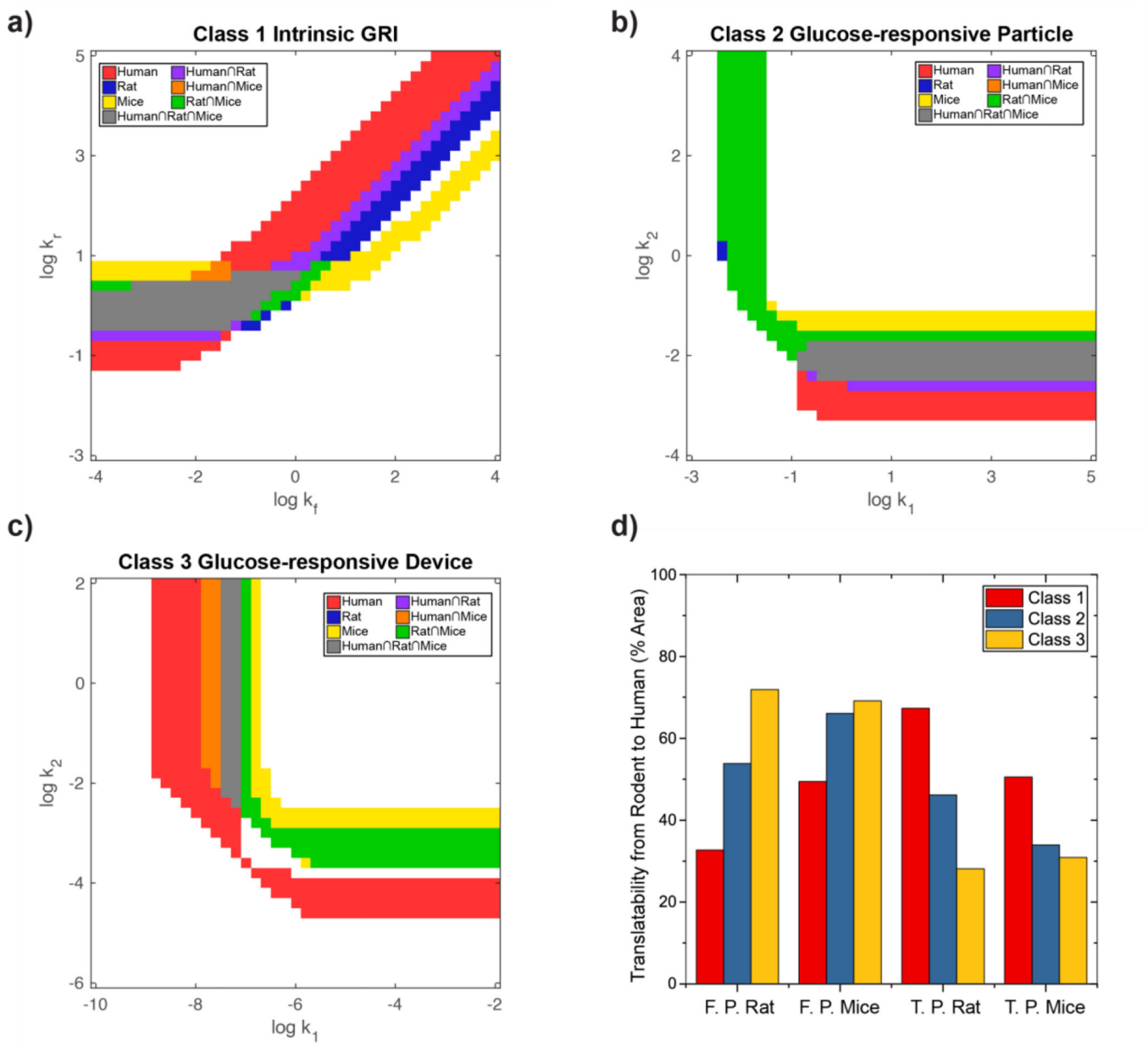

Figure 6.

Interspecies translatability evaluation of class 1, 2, and 3 GRIs. a-c) Projected two-dimensional parametric efficacy plot of a) iGRIs, b) GRPs, and c) GRDs. For iGRIs, forward (k_f) and backward (k_b) rate constants are chosen as design parameters. GRI activation reaction constant (k_1) and insulin releasing rate constant (k_2) are used to map GRPs and GRDs. Purple, orange, and gray-colored regions are overlapped areas between humans and rodents, respectively, indicating that success in animal experiments would be successfully translated to clinical trials. Blue and yellow-colored regions are rodent-only areas, which indicates success in animal experiments may not be successful in the human clinical trial. The red-colored region is the human-only area, which means therapeutics with unsuccessful animal experiments may be efficacious in a human trial. d) False positive and true positive

area fraction of GRIs from rodents to humans. The true positive is defined as the area overlapping with both humans and rodents divided by the area of rodents. The false positive is defined as the area only for rodents divided by the whole area of rodents.